Annals of Biomedical Engineering, Vol. 44, No. 12, December 2016 *(© 2016)* pp. 3619–3631
DOI: 10.1007/s10439-016-1672-9

Reduced-Dimension Modeling Approach for Simulating Recruitment/De-recruitment Dynamics in the Lung

JASON RYANS,[1] HIDEKI FUJIOKA,[2] DAVID HALPERN,[3] and DONALD P. GAVER[1]

[1]Department of Biomedical Engineering, Tulane University, 534 Lindy Boggs Building, New Orleans, LA 70118, USA; [2]Center for Computational Science, Tulane University, New Orleans, LA, USA; and [3]Department of Mathematics, University of Alabama, Tuscaloosa, AL, USA

(Received 20 February 2016; accepted 2 June 2016; published online 8 June 2016)

Associate Editor Aleksander S. Popel oversaw the review of this article.

Abstract—Acute respiratory distress syndrome is a pulmonary disease that requires the use of mechanical ventilation for patient recovery. However, this can lead to development of ventilator-induced lung injury caused by the over-distension of alveolar tissue and by the repetitive closure (de-recruitment) and reopening (recruitment) of airways. In this study, we developed a multi-scale model of the lung from a reduced-dimension approach to investigate the dynamics of ventilation in the lung during airway collapse and reopening. The model consisted of an asymmetric network geometry with 16 generations of liquid-lined airways with airflow driven by a variable pleural pressure. During the respiratory cycle changes in airway radii and film thickness yield the formation of liquid plugs that propagate and rupture throughout the airway network. Simulations were conducted with constant surface tension values $15 \leq \gamma \leq 25$ dyn/cm. It was observed that the time onset of plug creation and rupture depended on the surface tension, as well as the plug aggregation/splitting behavior at bifurcations. Additionally, the plug propagation behavior was significantly influenced by presence of plugs in adjacent airways (i.e. parent and daughters) that affected the driving pressure distribution locally at bifurcations and resulted in complex aggregation and splitting behavior. This model provides an approach that has the ability to simulate normal and pathophysiological lung conditions with the potential to be used in personalized clinical medicine.

Keywords—Airway reopening, Ventilator-induced lung injury, Liquid plug, Mechanical ventilation, Reduced-dimension model.

Address correspondence to Donald P. Gaver, Department of Biomedical Engineering, Tulane University, 534 Lindy Boggs Building, New Orleans, LA 70118, USA. Electronic mail: dpg@tulane.edu

INTRODUCTION

Acute respiratory distress syndrome (ARDS) is a pulmonary disease that causes a degradation of the micro-mechanical environment of the lung. Pathological changes associated with ARDS include breakdown of the epithelial cell lined-lumen of the airways, surfactant deactivation, fluid accumulation in the lung, and the release of pro-inflammatory biomarkers.[23] These pathological changes can lead to impaired gas exchange and decreased patency throughout the respiratory bronchioles and alveoli. Mechanical ventilation is typically used as a treatment for ARDS, yet this method can exacerbate the conditions of the lung resulting in ventilator-induced lung injury (VILI). VILI is typically characterized by two primary mechanisms of damage consisting of over-distention of the lung tissue (volutrauma) and the repeated opening and closing of fluid-filled or collapsed airways (atelectrauma).[19]

During volutrauma, alveolar tissue is stretched beyond its equilibrium state such that the thin alveolo-capillary barrier is disrupted resulting in fluid leakage, reduced gas exchange, and inflammatory signaling. As a preventative measure, mechanical ventilation at low tidal volumes can mitigate the effects volutrauma. However, a deficiency in this implementation is that ventilation at lower tidal volumes can cause the repetitive collapse, or "de-recruitment" and reopening, or "recruitment", of pulmonary airways.[1] The cyclic de-recruitment and recruitment of airways can create microbubble and interfacial flows that transduce mechanical forces to the airway lumen resulting in cellular necrosis as demonstrated by several investigators using *in vitro*[13] and in silico models.[7,20,25]

The computational investigation of airway recruitment and de-recruitment events have been conducted

in single airway and simple network models. For example, Gaver *et al.*[10] demonstrated the theoretical mechanical implications of a finger of air propagating through a single fluid-filled and compliant airway. Additionally, Tai *et al.*[20] conducted direct numerical simulations of a single airway model to study the instability of the liquid-lining fluid and the flow-induced stresses on the airway lumen. While these and many other studies have elucidated varying phenomena occurring during airway reopening at the airway scale, there are still many queries as to how these mechanisms affect the lung at an anatomically relevant scale. Performing a direct numerical simulation of the Navier–Stokes equations to describe plug propagation and multiphase flow throughout an anatomically realistic network would be arduous to calculate and is, therefore, impractical. A more attractive alternative would be to use a reduced-dimension analysis to study the complex multi-physics and multi-scale interactions. Investigators such as Florens[6] and Tawhai[21] have made significant progress in the development of full-scale anatomically based airway models, yet these studies have not assessed the implications of liquid plug dynamics within these networks.

To achieve a better understanding of how to effectively implement mechanical ventilation strategies it is important to understand how liquid plug dynamics affect the overall ventilation of lung. In the current study, our goal is to simulate a dimensionally reduced airway network that incorporates the intricacies of local liquid plug dynamics to elucidate the global ventilation behavior of the lung.

MATERIALS AND METHODS

Conceptual Formulation

Conceptual Framework

We developed a rational engineering design approach for understanding the relationship between airway/alveolar recruitment and/or over-distension, and the mechanical stresses that damage sensitive pulmonary tissue in VILI. Due to the complexity of the system, we used a reduced-dimension approach to represent the behavior of the airways and alveoli during ventilation informed by higher order multiphase flow and fluid–structure interaction models. The framework for this simulation approach is based upon two components:

1. Fluid Components (FC) representing liquid occlusions in the form of long closure plugs or short liquid bridges, and
2. Tissue Components (TC) representing series and parallel segments of airways and alveoli.

FCs are created/destroyed and propagate based upon multiphase flows governed by local pressure distributions and physico-chemical properties. Simultaneously, TCs will respond to the local stress-field as determined by fluid–structure interactions. These may be damaged through over-distension (volutrauma) or the passage of a FC (atelectrauma). This process iterates in time, driven by system pressures that are dictated by flow from a mechanical ventilator.

The overall framework for the time-dependent simulation is shown in Fig. 1, which describes some of the primary mechanical interactions involved during respiration as well as the iterative process in which the bifurcation pressure (P_{BIF}) distribution is obtained. Note that the focus of this study is on mechanical interactions, though clearly the biological interactions will be critical to elucidating disease progression and may, in turn, affect the mechanical state of the system. However, in this first approach to a multi-scale model we include only the effects related to recruitment and de-recruitment of atelectic airways and the strain of open airways and alveoli. As described below, this model is intended to provide a quantitative link between mechanical events at the micro-scale of the peripheral airway and the macro-scale of the whole lung from which more robust and physiologically realistic models can be developed.

'Simple' Representation of FC/TC Interaction

To illustrate the concept of a fluid and tissue component interaction, consider the presence of a single liquid plug within a compliant airway surrounded by parenchymal connective tissue as seen in the FC of Fig. 2.

The motion of the plug within the airway contains an array of complex interactions, yet there are fundamental parameters that are of significant importance. For instance, the speed of the plug (U_{plug}) can be conceptually be expressed as a function of these particular parameters as

$$U_{plug} = F(\mu, \gamma, R, L, \Delta P, P_{ext}) \quad (1)$$

where μ is the viscosity, γ is the surface tension, R is the airway radius, L is the plug length, ΔP is the pressure drop in the airway, and P_{ext} is the external effective pressure due to the parenchymal tissue.

In this case, the function F can be considered a collection of state space variables whose interactions will determine the current state of the plug speed. These interactions are informed by previous plug

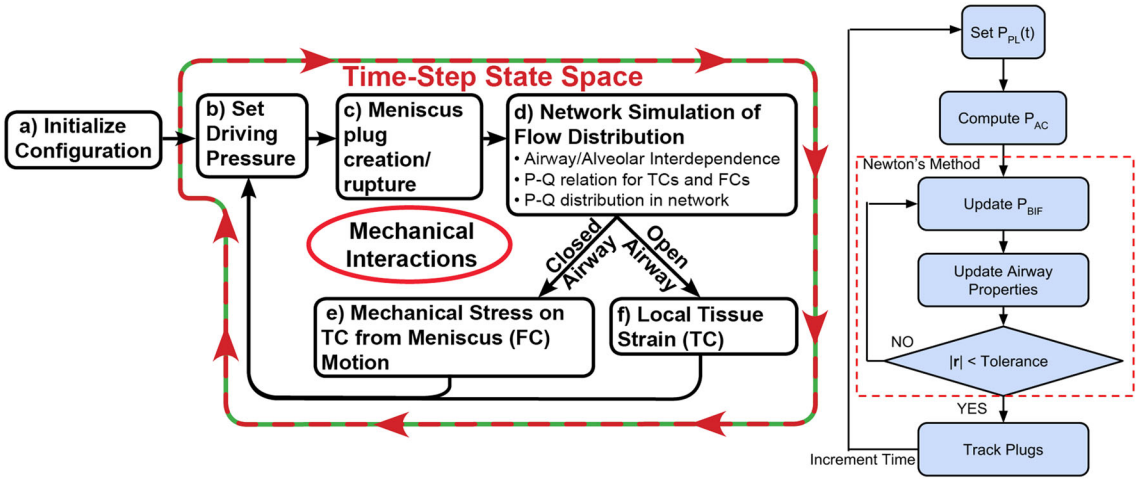

FIGURE 1. Schematic description of time stepping process and truncated algorithm flowchart.

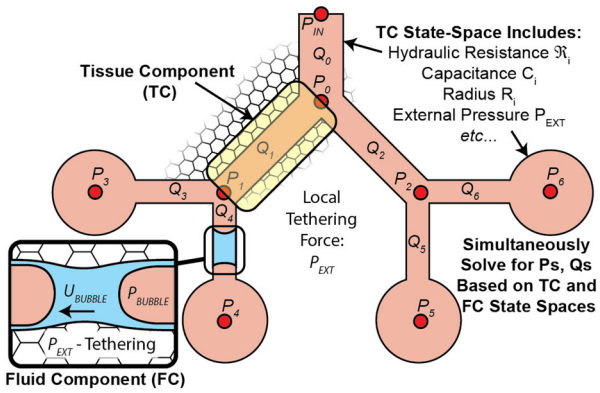

FIGURE 2. Schematic of network flow model.

propagation models[7,25] and can then be prudently incorporated into the reduced dimension lung model.

Conceptual Representation

To formalize the model using the approach above, we quantitatively specify the physical and interconnections between components, and the relationships between these components. We express the state space S^{TC} for each airway or acinar component as a function of an array of properties. The FC is one of TC's properties, which is represented by the state space S^{FC}. For example, S^{FC} for the airway 1 in Fig. 2 is

$$S^{TC}_{AW1} = F(a_1, L_1, P_0, P_1, P_{PA1}, Q_1, C_1, \gamma_1, \mu_1, \varepsilon_1, \cdots, F_{tube1}, S^{FC}_1) \quad (2)$$

where a_1, and L_1 represent the radius and length, P_1 and P_0 represent the internal pressures at both ends, P_{PA1} is the peri-airway pressure that relates to the state space of surrounding acini, S^{TC}_{AC}, γ_1, and μ_1 represent the surface tension and viscosity, Q_1 is the local flow-rate with $Q_1 = C_1(P_0 - P_1)$, ε_1 is the liquid film thickness, C_1 is the flow conductance (inverse of resistance) that depends on a_1, L_1, μ_1, ε_1, S^{FC}. F_{tube1} is the tube-law function that determines a_1 as a function of P_0, P_1, P_{PA1}, γ_1, and ε_1. S^{FC} may be a zero-length vector if no plug exists. It is also possible to have multiple plugs in the same airway.

The TCs for the acini take the form

$$S^{TC}_{AC} = F(V, P_{AC}, \ldots, F_{PV}) \quad (3)$$

where V is the volume of acini that is related to P_{AC} by the pressure–volume (PV) function F_{PV}. FC is created when the film thickness in S^{TC}_{AW} exceeds the critical value (e.g. $\varepsilon_{crit} = 0.12$). Also it is created when plug enters from other airway. It is destroyed when a plug ruptures or exits from the airway. The FCs are of the form

$$S^{FC} = F(x, L_P, U, \Delta P, \gamma, \mu, \cdots, F_{resistance}) \quad (4)$$

where x is the position of the plug within the airway, L_P and $U = Q/\pi a^2$ are the length and velocity of the plug, ΔP is the pressure difference across the plug, γ, and μ represent the surface tension and viscosity, and $F_{resistance}$ is the plug flow resistance that is a function of L_P, U, γ, μ.

System Evolution

The key to the modeling approach is the evolution of the state space as it depends upon each of the other components. To evolve the system, we increment the state space in time with a small time step Δt from a current state; for example, V of S^{TC}_{AC} is updated by $V(t + \Delta t) = V(t) + Q\Delta t$ and x of S^{FC} is updated by $x(t + \Delta t) = x(t) + U\Delta t$. Other state variables must be updated accordingly, which we conceptually define as a

differential algebraic equation $\mathbf{M}d\mathbf{S}/dt = \mathbf{G}(\mathbf{S})$ where **M** and **G** are a matrix and function of the state space components that define the network structure (connectivity) and the system governing equations that define reduced dimension interrelationships. This interaction can be quite intricate—for example, a change in the internal pressures will propagate through the system and change the external pressures and radius, thus driving flow (Q) and moving plugs.

Modeling Implementation

Modeling Overview

To investigate the mechanical interactions related to the heterogeneous ventilation and plug propagation behavior of the airway model, the algorithm introduced in Fig. 1 will be used to simulate whole lung respiration. Initially the time-dependent pleural pressure (P_{PL}) is set at the beginning of each time step. This provides the driving pressure for ventilation, as exists for normal respiration. Subsequently, the acinar pressures are evaluated using the PV relationship from Fujioka *et al.*,[8] and for spontaneous breathing the inlet pressure is set to atmospheric. Through an iterative procedure using Newton's method, the flow conductance and pressure drop for all airways is evaluated to compute the flow rate $Q = C\Delta P$. The pressure distribution through the network is updated based on the flow rate residual at each bifurcation to satisfy conservation of mass. The update of the airway pressure will change the airway radii, acinar volume, and airway film thickness with a tube law. This can yield the formation of liquid plugs from the lining liquid and the volume is maintained to satisfy conservation of mass. Since these updates will change the flow rates in the system, the iterative process continues until the flow rate residual $|r| < 10^{-7}$. Upon completion of the iterative process, the plug position is updated and the plug gains/deposits liquid from/to the lining liquid film depending on the capillary number (Ca) and the precursor film thickness (h_f). The time step is then incremented by small $\Delta t = 10^{-4}$s and the entire process is repeated. The following sections will outline the various implementation methods of the models described above. Note that while each section describes details of a particular method, there is a large degree of connectivity between one another.

Airway Morphology

The domain of the lung consists of an asymmetric network of airways up to an equivalent Weibel 16th generation consisting of $2^{16} = 65{,}526$ airways that terminate into acinar lobes. The morphology of the pulmonary airways was replicated from Lambert *et al.*[16] to describe the airway radius and length. A completely symmetric model with no gravitational effects would result in homogenous ventilation with all airways of the same generation collapsing simultaneously, with the smallest airways collapsing first. For this reason, we elected to introduce geometric asymmetry to our model; alternatively, asymmetry could be implemented in a symmetric tree through variation of airway film thickness, surface tension, compliance, or pleural pressure.

To induce asymmetry into the lung model, a symmetric seeding is created for 2^n airways. Terminal airway sisters are randomly chosen and appended to another randomly selected terminal airway. This pruning process is repeated for 2^{n-1} iterations, recognizing that newly appended sister airways are considered terminal airways, as is demonstrated by a diagram of a small section of the full model shown in Fig. 3. We used a Horsfield nomenclature[14] to articulate the asymmetric properties of the geometry beginning from the terminal airways. However, this approach does not replicate the precise geometries specified by Horsfield's analysis.

Once the asymmetric network is generated, the radius and length information for each airway is updated based on its equivalent Weibel generation number. Both the radius and length are a function of the Weibel generation number and is interpolated from Lambert *et al.*[16] Since this previous study only provides data up the 16th Weibel generation and the result of inducing asymmetry can yield terminal airways with larger equivalent Weibel generations, the representation is scaled so that all of the terminal airways have the identical geometries that terminate with acinar lobes that have mechanical properties described in "Acinar Pressure–Volume Relationship".

Acinar Pressure–Volume Relationship

The morphological information of the representative acinar regions connected to the terminal airway of the lung is based on the octahedral models depicted in Fujioka *et al.*[8] The characteristics of this acinar model are governed by the PV relationship expressed as

$$\frac{V}{V_{FRC}} = a + \frac{b}{1 + \exp[(\Delta P - c)/d]} \tag{5}$$

where V is the acinar volume, V_{FRC} is the acinar volume at FRC, ΔP is the transpulmonary pressure, and a–d are constants for fitted curves that describe the mechanical characteristics of the surrounding parenchyma.

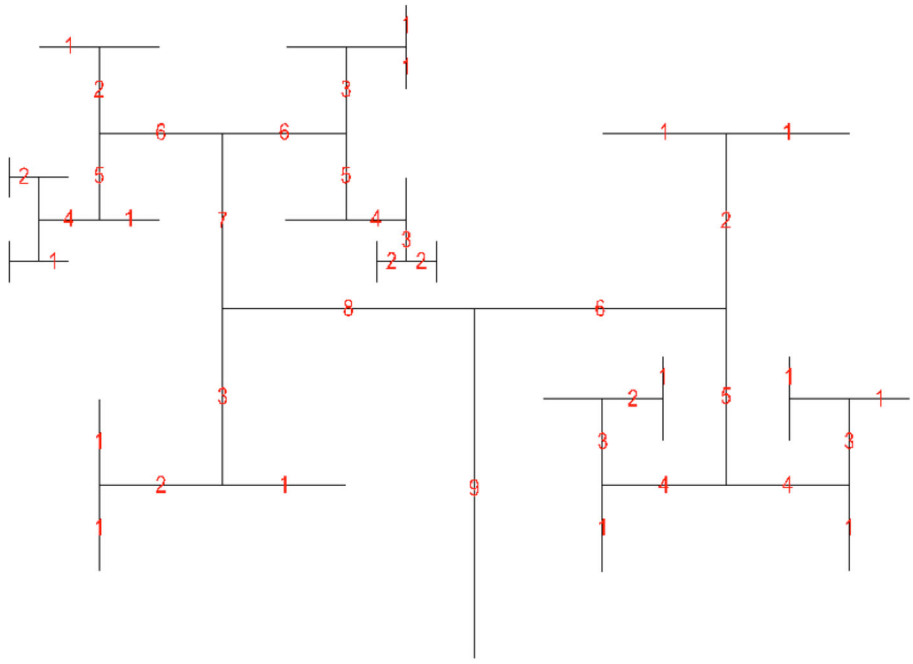

FIGURE 3. Graphical representation of a portion of the airway network (Horsfield nomenclature).

Tube Law

To describe the fluid–structure interactions of the airway wall during ventilation a tube law was utilized that changed the radius of the airway lumen over time as a function of the transmural pressure. The transmural pressure acts across the wall of the airway and can be defined as

$$P_{TM} = P_{int} - P_{ext} \tag{6}$$

where P_{TM} is the transmural pressure, P_{int} is the pressure within the airway, and P_{ext} is the exterior pressure. The pressure within the airway is subject to the upstream and downstream pressures at either end of the airway as well as the Laplace pressure from the liquid lining of airway. The average pressure from that at both ends of the airway and the Laplace pressure can be expressed as

$$P_{int} = P_{AW} - \gamma/R_{in} \tag{7}$$

$$P_{AW} = \frac{P_{UP} + P_{DN}}{2} \tag{8}$$

where P_{UP} is the upstream pressure, P_{DN} is the downstream pressure, P_{AW} is the average airway pressure, γ is the surface tension of the liquid lining, R_{in} is the radius from the centerline of the airway to the liquid lining. The pressure outside of the airway is governed by the pleural pressure (P_{PL}), which is prescribed by a sinusoidal waveform that varies between -2 cmH_20 and -10 cmH_20 with a period of 5 s. This waveform is intended to replicate the pleural pressure variation during a single respiratory cycle at normal conditions. However, it should be noted that since there are no gravitational effects in the model that the pleural pressure is the same throughout the entire network. From Eq. (6) and (7) the transmural pressure can be rewritten as

$$P_{TM}(t) = P_{AW} - P_{PL}(t) - \gamma/R_{in}(t) \tag{9}$$

where the transmural pressure varies with time due to the sinusoidal nature of the pleural pressure and changes the airway radius (Fig. 4a).

Airway Liquid Lining

The liquid lining of the airways was prescribed initially to be 10 μm uniformly distributed throughout the length of each airway.[24] As the radius of the airway changes over time, consequentially of the tube law, the thickness of the liquid layer will also change. The ratio of the liquid thickness to that of the airway radius is defined as

$$\varepsilon = \frac{R_{out} - R_{in}}{R_{out}} \tag{10}$$

where R_{out} is the airway radius and R_{in} is the radius from the centerline to the liquid layer (Fig. 4b). The ε of each airway is prescribed at the beginning of the simulation as the ratio of the initial liquid thickness and the maximum radius of the airway such that

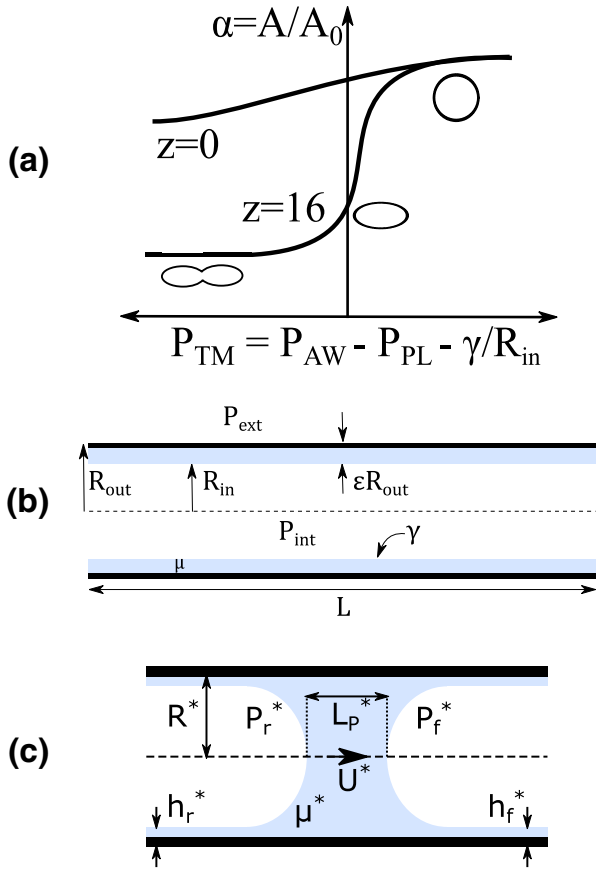

FIGURE 4. (a) Tube law at the trachea ($z = 0$) and an airway at the 16th generation ($z = 16$) (b) Airway liquid lining (c) Plug propagation simulation domain.

$$\varepsilon_0 = 10\ \mu\text{m}/R_{\text{out}} \tag{11}$$

As the radius of the airway decreases, ε will correspondingly increase and will eventually reach a critical value where instabilities of the liquid lining of the airway will cause a plug to form.[12] The critical value was $\varepsilon_{\text{crit}} = 0.12$. If $\varepsilon \geq \varepsilon_{\text{crit}}$, we assume that an obstruction (liquid-bridge) spontaneously forms[9] (see "Liquid Plug Flow" section) at the center of the airway.

Liquid Plug Flow

In order to model multiple plugs moving within an airway tree from a reduced dimension approach, a set of simplified formulas were developed that are based on full CFD computational simulations of micro-scale models of plug propagation as described in the Supplemental Material. These formulas describe the flow resistance caused by liquid plug propagation as a function of the plug length, capillary number, and the precursor film thickness. The formulas were based on computational investigations of three key contributors to the plug resistance: the front meniscus, the plug core, and the rear meniscus. This is expressed as

$$\Delta P^*_{\text{plug}} = S^*_{\text{plug}} Q^*_{\text{plug}} \tag{12}$$

$$S^*_{\text{plug}} = S^*_f + S^*_r + S^*_c \tag{13}$$

where ΔP^*_{plug} is the pressure drop due to the plug, S^*_{plug} is the plug resistance, Q^*_{plug} is the plug flow rate, S^*_f is the resistance due to the front meniscus of the plug, S^*_r is the resistance due the rear meniscus of the plug, and S^*_c is the resistance due the viscous core. This is used to prescribe the pressure drop in an airway due to the propagation of a liquid plug. For validation, the results from these formulas were compared to full CFD investigations and demonstrated faithful representation.

Flow Dynamics

Airflow throughout the lung model is described using a Poiseuille relationship at each bifurcation, with each parent airway always splitting into two daughter airways (Fig. 5a).

Flow rates within the parent and daughter airways can be respectively defined as

$$Q_{\text{P}} = C_{\text{P}}(P_{\text{B}} - P_{\text{P}}) \tag{14}$$

$$Q_{\text{D},i} = C_{\text{D},i}(P_{\text{D},i} - P_{\text{B}}) \tag{15}$$

where Q_i is the flow rate of the airway, C_i is the conductance of the airway, and P_i is the corresponding bifurcation pressure. In this scenario, flow is conserved at each bifurcation point and is driven by the pressure drop between each bifurcation.

With the flow behavior between a parent and set of daughter airways defined, this can be extrapolated to the entire airway network. Assuming that there are N_{b} number of bifurcations, N_{aw} number of airways, and N_{ac} number of acini, the pressure difference in each airway can be prescribed by

$$\overrightarrow{dp} = \mathbf{D}\overrightarrow{p} + \overrightarrow{d_t}P_{\text{T}} + \mathbf{D}_{\text{AC}}\overrightarrow{P_{\text{AC}}} \tag{16}$$

where P_{T} is the pressure at the inlet of the trachea, $\overrightarrow{d_t}$ is the time derivative, P_{AC} is the acinar pressure, $\boldsymbol{D}$ is a $N_{\text{aw}} \times N_b$ parent-daughter connectivity matrix, $\overrightarrow{p}$ is a $N_b \times 1$ vector of node pressures at bifurcations, and $\overrightarrow{dp}$ is a $N_{\text{aw}} \times 1$ vector of pressure differences at each airway. With Eq. (16) the flow rate of the airways can defined similarly to Eqs. (14) and (15) as

$$\overrightarrow{q} = \mathbf{C}\overrightarrow{dp} = \mathbf{C}(\mathbf{D}\overrightarrow{p} + \overrightarrow{d_t}P_{\text{T}} + \mathbf{D}_{\text{AC}}\overrightarrow{P_{\text{AC}}}) \tag{17}$$

where $\overrightarrow{q}$ is a $N_{\text{aw}} \times 1$ vector of flow rates, Q in the airways, and $\mathbf{C}$ is a $N_{\text{aw}} \times N_{\text{aw}}$ matrix of airways conductance, C.

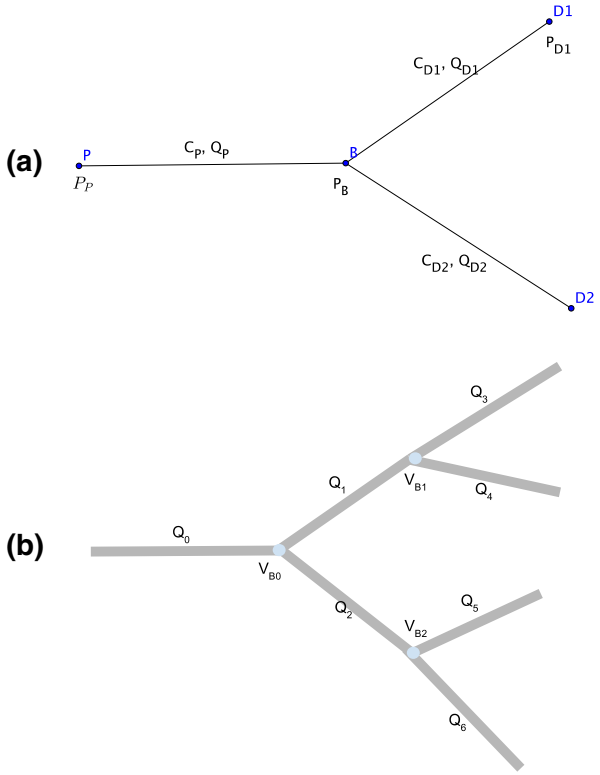

FIGURE 5. (a) Parent and daughter airway connectivity (b) Plug propagation in airway network.

In order to conserve mass at each bifurcation point the flow residual should be zero such that

$$\vec{r} = \mathbf{B}\vec{q} = 0 \tag{18}$$

where $\vec{r}$ is a $N_b \times N_{\text{aw}}$ vector of flow rate residual and $\mathbf{B}$ is a $N_b \times N_{\text{aw}}$ matrix. The bifurcation pressures are iteratively solved for by Newton's method where small perturbations of $\vec{p}$ will change $\vec{r}$ such that

$$\vec{r} = \mathbf{B}\vec{q} = \mathbf{BC}(\mathbf{D}\vec{p} + \vec{d}_t P_T + \mathbf{D}_{\text{AC}}\overrightarrow{P_{\text{AC}}}) \tag{19}$$

Assuming that the airway conductances are constant for small perturbations in $\vec{p}$,

$$\partial\vec{r} \approx \mathbf{BCD}\partial\vec{p} \tag{20}$$

where $\mathbf{BCD}$ is a $N_{\text{b}} \times N_{\text{b}}$ matrix. For given pressures at bifurcations, $\vec{p_0}$, the flow rate residuals, $\vec{r}(\vec{p_0})$, are computed. If $\left|\vec{r}(\vec{p_0})\right| \leq 10^{-7}$, then the iteration is exited. Otherwise, the following linear system is solved

$$\mathbf{BCD}\vec{x} = \vec{r}(\vec{p_0}) \tag{21}$$

where $\vec{x} = \vec{p_0} - \vec{p}$ and $\vec{p_0}$ is updated with $\vec{p}$.

Liquid Plug Kinematics

To observe the dynamic behavior that airway recruitment and de-recruitment have on lung ventilation, the movement of the liquid plugs must be carefully tracked throughout the airway network. To accomplish this, we initially assume that when a plug forms in an airway it does so at the center position of the given length of the airway. According to the mechanics of the liquid plug flow mentioned earlier, as the plug propagates through an airway it will leave behind a trailing film of liquid and will accumulate liquid in front of it from the precursor film. There are two mechanisms for plug clearance, the first of which occurs when the length between the two menisci of the plug becomes zero due to loss of plug volume during propagation. The second method of clearance is when a plug travels to the acinus at the end of a terminal airway. In this scenario we assume that liquid entering the acinus is immediately reabsorbed effectively leaving the acinus with no volume from the liquid plug. This is based on studies[22] that have shown that alveoli have membrane proteins, known as aquaporin, that facilitate fluid transport from the airspace based on osmotic pressure gradients. Since the rate at which this clearance occurs is still not fully understood and depends on may biological factors, we have idealized the clearance occurred instantaneously when a plug entered the acinus.

In addition to formation and clearance, liquid plugs also have the ability to split and join at bifurcations through the airway tree. It should be noted that in this meso-scale model the micro-scale geometric characteristics of bifurcations are not explicitly defined. Therefore, plugs cannot rupture at bifurcations. However, the volume ratio at which plugs split at a bifurcation is proportional to the relative flow rates from the corresponding parent and daughter branches. This response helps to dissipate a plug in the vicinity of a bifurcation.

For example, Fig. 5b illustrates a possible scenario of plugs moving through the airway network and encountering different bifurcations. We define the flow rates of each airway as

$$\Phi = \begin{bmatrix} -Q_0 & 0 & 0 \\ Q_1 & -Q_1 & 0 \\ Q_2 & 0 & -Q_2 \\ 0 & Q_3 & 0 \\ 0 & Q_4 & 0 \\ 0 & 0 & Q_5 \\ 0 & 0 & Q_6 \end{bmatrix} \tag{22}$$

where Φ is a $N_{\text{aw}} \times N_b$ matrix and each element $\Phi(i,j)$ is the flow rate in each airway, with each column representing the conservation of flow at each bifurcation. With the ℓ_1 norm, defined as $\phi_j = \Sigma_i \Phi_{ij}$, the normalized Φ can be expressed as

$$\tilde{\Phi} = \begin{bmatrix} -Q_0 & 0 & 0 \\ Q_1 & -Q_1 & 0 \\ Q_2 & 0 & -Q_2 \\ 0 & Q_3 & 0 \\ 0 & Q_4 & 0 \\ 0 & 0 & Q_5 \\ 0 & 0 & Q_6 \end{bmatrix} \begin{bmatrix} 1/\phi_0 & 0 & 0 \\ 0 & 1/\phi_1 & 0 \\ 0 & 0 & 1/\phi_2 \end{bmatrix} = \begin{bmatrix} -Q_0/\phi_0 & 0 & 0 \\ Q_1/\phi_0 & -Q_1/\phi_1 & 0 \\ Q_2/\phi_0 & 0 & -Q_2/\phi_2 \\ 0 & Q_3/\phi_1 & 0 \\ 0 & Q_4/\phi_1 & 0 \\ 0 & 0 & Q_5/\phi_2 \\ 0 & 0 & Q_6/\phi_2 \end{bmatrix} \tag{23}$$

For example, at bifurcation 0 the liquid bolus of volume V_{B0} will be distributed into the parent airway ($V_{B0}(-Q_0)/\phi_0$), and each of the daughter airways ($V_{B0}(-Q_1)/\phi_0$ and $V_{B0}(-Q_2)/\phi_0$) for airway 0,1, and 2 respectively. In general, the volume of the liquid plug that gets into each airway (V_{Pi}) can be computed by

$$\begin{bmatrix} V_{P0} \\ V_{P1} \\ V_{P2} \\ V_{P3} \\ V_{P4} \\ V_{P5} \\ V_{P6} \end{bmatrix} = \begin{bmatrix} -Q_0/\phi_0 & 0 & 0 \\ Q_1/\phi_0 & -Q_1/\phi_1 & 0 \\ Q_2/\phi_0 & 0 & -Q_2/\phi_2 \\ 0 & Q_3/\phi_1 & 0 \\ 0 & Q_4/\phi_1 & 0 \\ 0 & 0 & Q_5/\phi_2 \\ 0 & 0 & Q_6/\phi_2 \end{bmatrix} \begin{bmatrix} V_{B0} \\ V_{B1} \\ V_{B2} \end{bmatrix} \tag{24}$$

The value of Q_i must satisfy conservation of mass following "Flow Dynamics" section.

RESULTS

In this study, a sinusoidal pleural pressure was applied to drive respiration with $-10 \leq P_{PL} \leq -2$ cmH_2O and a frequency of $f = 12$ min^{-1}. For each simulation the surface tension is held constant throughout the respiratory cycle with $15 \leq \gamma \leq 25$ dyn/cm. While this does not reflect the dynamic behavior of surface tension during respiration, it can still provide valuable insight into the interrelationship between surface tension and airway recruitment/de-recruitment. We define low, medium, and high surface tension values to be 15, 20, and 25 dyn/cm, respectively.

To describe the evolution of the system, Fig. 6 illustrates the general progression of plug formation, movement, and clearance during the respiratory cycle. In Fig. 6a, the radii of the airways is continually decreasing during the expiration phase due to the tube law and subsequently causes an increase in ε. Just before the end of expiration, seen in Fig. 6b, $\varepsilon \geq \varepsilon_{crit}$ causes an instantaneous formation of plugs within the center of airways. It should be noted that this approximation of the position of plug creation could affect the residence time and propagation behavior of the plug. After formation, the plugs propagated either towards the upper airways or the acini depending on current state of the driving pressure gradient. Figure 6c shows the splitting of a plug from a parent to the daughter branches, as well as the clearance of plugs into connected acini.

To investigate the dynamics of airway recruitment and de-recruitment within the lung, as well as elucidate behavior of plug propagation, throughout a respiratory cycle the aggregate number of plugs present in airways was recorded. Additionally, the position of each plug was tracked as it traversed the airways. Figure 7 illustrates the number of total plugs present in the lung during a respiratory cycle from creation to rupture. From this information, there are two specific signature characteristics that can be investigated to elucidate plug propagation behavior and airway recruitment/de-recruitment.

The first signature characteristic observed is the time onset and residence time of plug creation and rupture as it depends on the surface tension. For the low surface tension value, the residence time of the liquid plug was the smallest and this residence time increased as the surface tension increased. Additionally, with large γ the plug forms earlier in the respiratory cycle and ruptures later in the cycle. It should be noted that surface tension values below 15 dyn/cm resulted in no plugs forming during the respiratory cycle, and surface tension values above 25 dyn/cm resulted in plugs forming in multiple generations near the terminal airways without the ability to propagate.

The second signature characteristic is the effect of surface tension on that of plug aggregation behavior. This is most clearly demonstrated in the case of the medium surface tension (green) illustrated in Fig. 7. In this case, liquid plugs are formed in only the terminal airways similar to that of the low surface tension value. However, unlike the low surface tension simulation that has plugs only moving in the terminal airways, the plugs in the medium surface tension simulation propagate initially towards the upper airways, causing them to aggregate at airway bifurcations. Once the respiratory cycle enters the inspiration phase, the plugs reverse direction towards the acini until they rupture. It should be noted that this plug aggregation behavior is also present in the high surface tension value, but is masked by the presence of

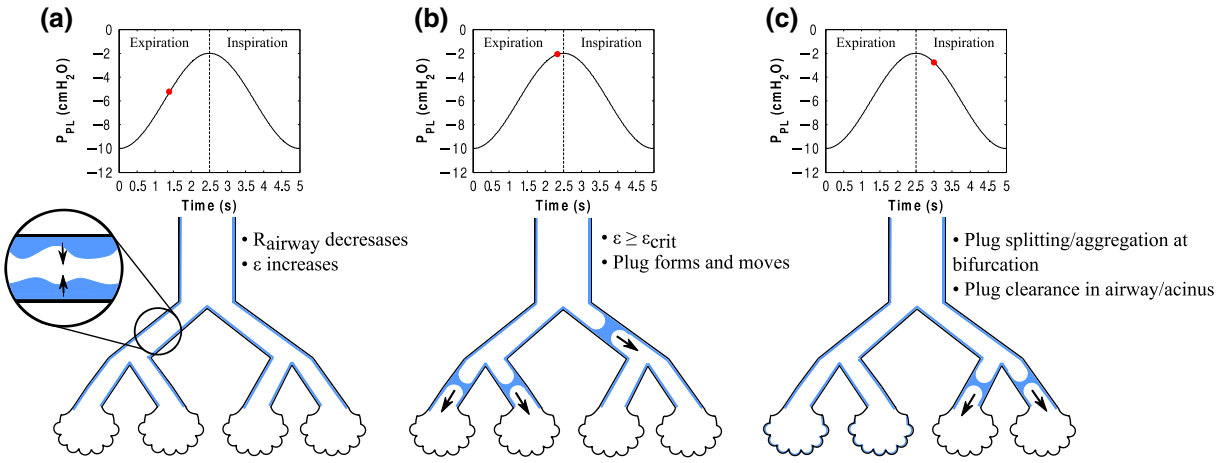

FIGURE 6. Progression of plug (a) formation, (b) propagation, and (c) clearance.

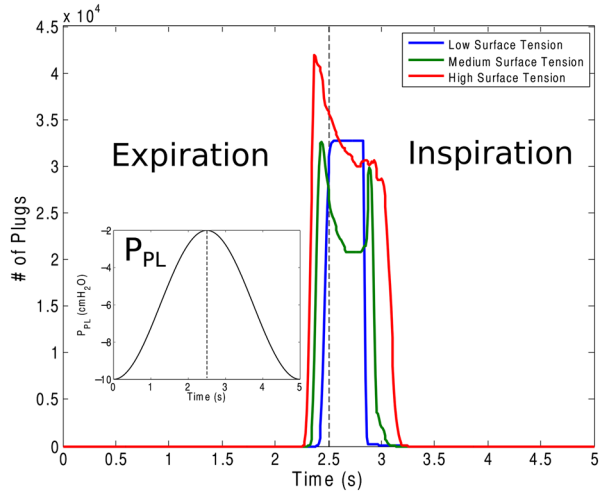

FIGURE 7. Number of plugs present in airway network during respiratory cycle.

more overall plugs and effects of interaction with neighboring plugs.

The plug propagation behavior during the respiratory cycle is influenced by two primary factors that include the airway network configuration and the presence of "nearest neighbor" plugs. Figure 8 illustrates some of the heterogeneous retrograde plug behavior seen at a single time point for a small section of the airway network. The black arrows depict plugs moving towards the upper airways, while red arrows represent plugs moving towards the acini.

A plug is considered in retrograde motion when it is traveling in the opposite direction of the macro flow pattern during either the expiratory or inspiratory phase. For instance, plugs that form towards the end of expiration before 2.5 s will be initially propagating towards the upper airways. Once the pleural pressure enters the inspiratory phase after 2.5 s, any plugs still propagating towards the upper airways are considered in retrograde motion. This retrograde behavior is further captured in Fig. 9, where the ratio of plugs traveling in retrograde motion is examined. From this it is observed that increased surface tension yields a longer transition time for all plugs to reverse direction when going from the expiratory to inspiratory phase. Additionally, increased surface tension yields more plugs upstream of the terminal airways. This leads to increased time in retrograde motion of plugs towards the terminal airways.

DISCUSSION

From the first signature of Fig. 7, there was a time lag associated with creation and rupture of liquid plugs as the surface tension was modified. The formation of plugs earlier in the respiratory cycle with increased surface tension can be explained by the effect transmural pressure has on the tube law as seen in Fig. 10. From Eq. (9), for a given pleural pressure the increase in the surface tension will reduce the transmural pressure and shift the airway to a more compliant state. For $\gamma < 15$ dyn/cm, plugs were not created during the respiratory cycle because the tube law did not yield a change in radius that resulted in $\varepsilon \geq \varepsilon_{crit}$. For $\gamma > 25$ dyn/cm, plugs were created in multiple generations near the terminal airways, but did not propagate because the driving pressure for the plugs was not sufficient enough to overcome the downstream resistance in the network. This implies that there might exist thresholds that govern plug creation and movement:

1. *Critical Surface Tension Threshold*—This is the surface tension value that is necessary for P_{TM}

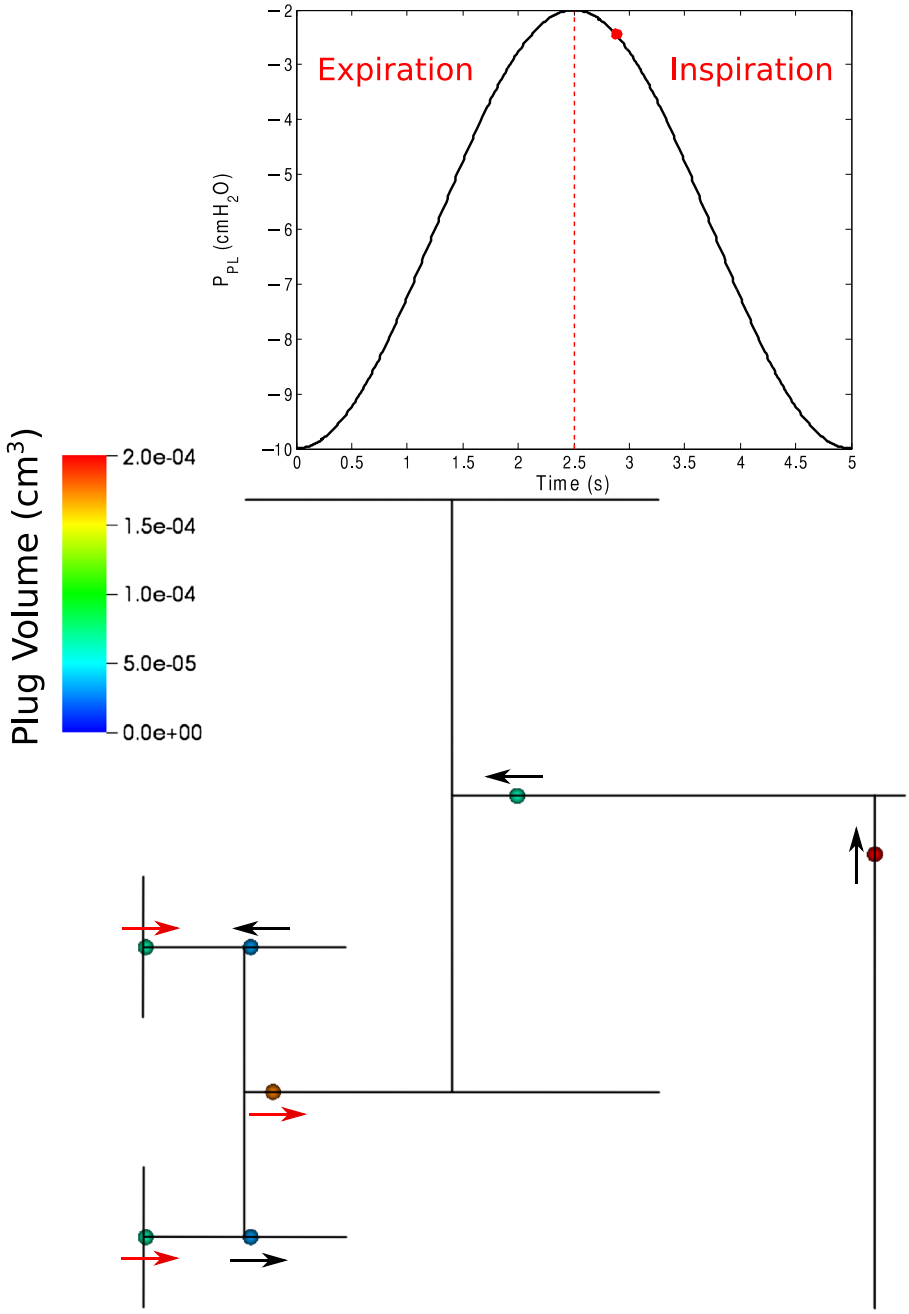

FIGURE 8. Plug propagation direction during inspiration at t = 2.74 s. Black arrows indicate retrograde motion towards upper airways. Red arrows show motion towards acini.

to be small enough to cause plug formation when $\varepsilon \geq \varepsilon_{crit}$.

2. *Yield Surface Tension Threshold*—This is the surface tension value that is needed for the driving pressure to overcome the effective airway resistance and begin the reopening process, as mentioned in previous studies.[11]

Additionally, this highlights the importance of pulmonary surfactant to reduce the surface tension at the air–liquid interface during respiration to prevent airway closure. This suggests that dynamic surface tension can protect the airways from obstructions by reducing γ below γ_{crit} and also may increase the likelihood of reopening by reducing the yield pressure.

The heterogeneous plug propagation behavior seen in Fig. 8 was largely attributed to not only the network configuration of the airway tree, but also the presence of plugs in adjacent airways (i.e. parent and daughters). The asymmetric geometrical configuration was a prominent factor in heterogeneous plug propagation

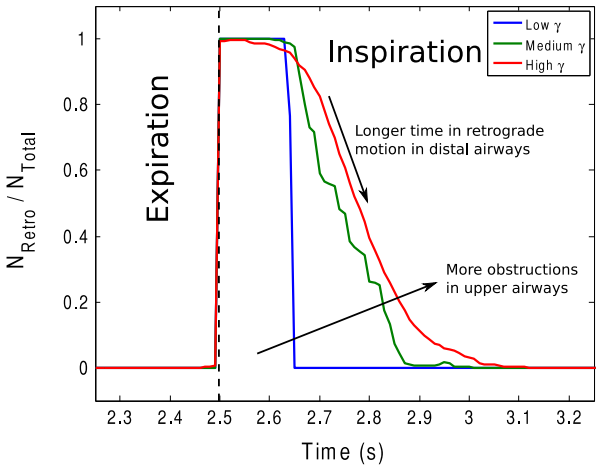

FIGURE 9. Ratio of plugs in retrograde motion.

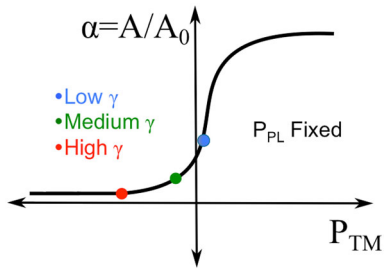

FIGURE 10. Tube law interrelationship between surface tension and transmural pressure.

because it influenced the global driving pressure distribution to move plugs throughout the airways. The driving pressure gradient was higher in airways that had shorter path lengths and thus created "paths of least resistance". This change in the global driving pressure distribution also has some inherent time lag associated with it has seen with the low γ case in Fig. 9. In this scenario all of the plugs in the system are created and only propagate in terminal airways. Once the respiratory cycle enters the inspiratory phase, there is a period of time where the plugs are in retrograde motion before reaching a driving pressure to reverse propagation direction. This phase shift of the driving pressure and plug flow is a result of the capacitive properties of the acini, similar to what is demonstrated in a RC circuit.

The presence of plugs in adjacent airways caused local pressure distribution changes that indirectly allowed adjacent plugs to communicate and influence their propagation behavior. This raises interesting questions about the effect that a rupturing plug has on the tendency for surrounding plugs to rupture. In Fig. 9 there appears to be acceleration in the rate at which plugs end retrograde motion and propagate towards the acini. Studies by Alencar *et al.*[2,3] have shown that these events could be related to avalanche reopening and crackles, where airways open in avalanches triggered by overcoming a hierarchy of critical opening threshold pressures along the airway tree. It was also observed that plugs in adjacent airways affected the driving pressure distribution locally at bifurcations and resulted in complex aggregation and splitting behavior. This is further seen in Fig. 11a where there are plugs in adjacent airways moving in opposite directions. In this case, plugs with a positive velocity are those moving towards the acini and those a negative velocity are moving towards the upper airways. Additionally, in Fig. 11b the internal airway pressure illustrates the local pressure distributions that drive plug flow.

The critical epsilon sensitivity was investigated by varying ε_{crit} by both $\pm 10\%$ and $\pm 25\%$ to determine its impact on the simulation behavior. We found that this modification exhibited predictable results by (a) decreasing plug residence time with increased critical value, and (b) increasing residence time with decreased critical value. Furthermore, the variations from the base critical epsilon value showed insignificant change in the plug residence time.

Understanding these mechanical interactions of respiration is especially important when attempting to model pathophysiological conditions. One example is the ability to mimic bronchoconstriction during asthma. Previous studies[4,5] have investigated modeling bronchoconstriction by relating stresses resulting from parenchymal tethering to the effective transmural pressure of an airway. While these models provide valuable quantitative insight into understanding this phenomenon, they do not incorporate the mechanical effects of flows occurring within the airway. It has been shown that airway mucus hyper-secretion is evident in many asthmatic patients and contributes to airway narrowing.[18] The presence of thicker mucus lined and/or plug filled airways is likely to have an effect on the transmural pressure that drives bronchoconstriction. Additionally, the mucosal edema present in airways could alter the viscosity and surface tension seen in normal physiology that could impact the mechanics of airway recruitment/de-recruitment. Coupling the effects of parenchymal tethering with that of the plug flow mechanics within this study would likely yield an improved approach to modeling bronchoconstriction during asthma.

Limitations

While this model provides a unique approach to coupling the various components of respiratory mechanics, some aspects represent idealized conditions that need to be improved upon in the future. In par-

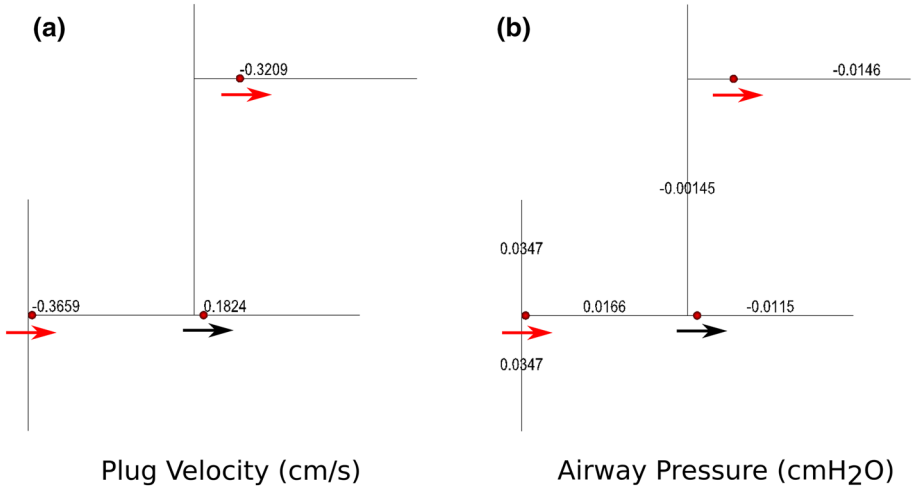

FIGURE 11. Retrograde plug motion in inspiratory phase shown by (a) plug velocity and (b) airway pressure.

ticular, this model does not currently incorporate the effects of gravity on plug propagation mechanics, mechanical interactions of airways and surrounding parenchymal connective tissue, and the kinematics that vary surface tension during the respiratory cycle. The gravitational effects will add another level of complexity that could affect plug propagation speed, plug aggregation/splitting, and the pleural pressure distribution throughout the airway tree.

To address the integration of mechanical interactions between airways and parenchyma, we will expound upon previous work by Fujioka *et al.*[8] that outlined a model developed for uniformly open airways/alveoli. It is well known that in disease states that some regions of the lung are ventilated, while other are ateletic. We will extend this work to our computational model to generate a physiologically realistic 3D lung airway/acinar network within lung lobes based on the algorithm proposed by Tawhai *et al.*[21] In conjunction, a more comprehensive model of lung airway compliance will be incorporated to better reflect the mechanics of airways during a diseased state in addition to the current tube law model.

To incorporate the presence of variable surface tension at the airway lumen interface during respiration, we will include a Langmuir kinetics model proposed by Otis *et al.*[17] This model will consider the transport of surfactant from the bulk solution to the interface based on surfactant multilayer theory similar to that of Krueger and Gaver.[15] Additionally, a more precise tube law will need to be utilized for airways beyond the conducting zone to better represent the behavior dynamic surface tension has on airway recruitment/de-recruitment. With all of these mechanics in place we will be able to adequately validate our modeling approach with experimental data, primarily by comparing the PV loop generated by our airway system with that of clinical results.

Conclusions

In this study we developed a reduced-dimension model of the lung to simulate the dynamics of airway closure and reopening due to liquid plug formation and clearance. The model consisted of an asymmetric network geometry with 16 generations of liquid-lined airways, and was mechanically coupled to the interactions of liquid plugs propagating through the airway tree during respiration. We were able to demonstrate the interrelationship between surface tension of the airway liquid-lining and the de-recruitment/recruitment of airways. Additionally, we investigated the plug propagation behavior as it relates to the geometrical morphology of the airway network, as well as the behavior of adjacent plugs.

Coupling our current model with parenchymal tethering effects would provide an ability to investigate the behavior of various pathophysiological conditions including ARDS, asthma, cystic fibrosis, emphysema, and bronchitis. Once the model can adequately imitate the desired pathophysiology, it will be possible to perform future simulations of mechanical breathing to elucidate the most effective mechanical ventilation treatment strategy. This is useful for not only ARDS, but for cystic fibrosis as well where there is a need currently for more effective ventilation therapies. Ideally, the model will act as a clinical tool that could be utilized for assessing treatment strategies with a personalized medicine ideology. This could be accomplished by using patient-specific morphological information acquired from the 3D reconstruction of radiological scans.

ELECTRONIC SUPPLEMENTARY MATERIAL

The online version of this article (doi: 10.1007/s10439-016-1672-9) contains supplementary material, which is available to authorized users.

ACKNOWLEDGMENTS

This study was supported by National Science Foundation Grant CBET-1033619 and Research Traineeship Grant DMS-1043626. Computational resources were supported in part using high performance computing (HPC) resources and services provided by Technology Services at Tulane University, New Orleans, LA.

REFERENCES

[1]Albert, S. P., J. DiRocco, G. B. Allen, J. H. Bates, R. Lafollette, B. D. Kubiak, J. Fischer, S. Maroney, and G. F. Nieman. The role of time and pressure on alveolar recruitment. *J. Appl. Physiol.* 106(757–765):2009, 1985.

[2]Alencar, A. M., S. V. Buldyrev, A. Majumdar, H. E. Stanley, and B. Suki. Avalanche dynamics of crackle sound in the lung. *Phys. Rev. Lett.* 87:088101, 2001.

[3]Alencar, A. M., A. Majumdar, Z. Hantos, S. V. Buldyrev, H. E. Stanley, and B. Suki. Crackles and instabilities during lung inflation. *Physica A* 357:18–26, 2005.

[4]Bates, J. H., and A.-M. Lauzon. Parenchymal tethering, airway wall stiffness, and the dynamics of bronchoconstriction. *J. Appl. Physiol.* 102:1912–1920, 2007.

[5]Breen, B. J., G. M. Donovan, J. Sneyd, and M. H. Tawhai. Quantifying parenchymal tethering in a finite element simulation of a human lung slice under bronchoconstriction. *Respir. Physiol. Neurobiol.* 183:85–90, 2012.

[6]Florens, M., B. Sapoval, and M. Filoche. An anatomical and functional model of the human tracheobronchial tree. *J. Appl. Physiol.* 110:756–763, 2011.

[7]Fujioka, H., and J. B. Grotberg. Steady propagation of a liquid plug in a two-dimensional channel. *J. Biomech. Eng.* 126:567–577, 2004.

[8]Fujioka, H., D. Halpern, and D. P. Gaver, 3rd. A model of surfactant-induced surface tension effects on the parenchymal tethering of pulmonary airways. *J. Biomech.* 46:319–328, 2013.

[9]Gauglitz, P., and C. Radke. An extended evolution equation for liquid film breakup in cylindrical capillaries. *Chem. Eng. Sci.* 43:1457–1465, 1988.

[10]Gaver, D. P., D. Halpern, O. E. Jensen, and J. B. Grotberg. The steady motion of a semi-infinite bubble through a flexible-walled channel. *J. Fluid Mech.* 319:25–65, 1996.

[11]Gaver, D., R. W. Samsel, and J. Solway. Effects of surface tension and viscosity on airway reopening. *J. Appl. Physiol.* 69:74–85, 1990.

[12]Hammond, P. Nonlinear adjustment of a thin annular film of viscous fluid surrounding a thread of another within a circular cylindrical pipe. *J. Fluid Mech.* 137:363–384, 1983.

[13]Higuita-Castro, N., C. Mihai, D. J. Hansford, and S. N. Ghadiali. Influence of airway wall compliance on epithelial cell injury and adhesion during interfacial flows. *J. Appl. Physiol.* 117(1231–1242):2014, 1985.

[14]Horsfield, K., G. Dart, D. E. Olson, G. F. Filley, and G. Cumming. Models of the human bronchial tree. *J. Appl. Physiol.* 31:207–217, 1971.

[15]Krueger, M. A., and D. P. Gaver. A theoretical model of pulmonary surfactant multilayer collapse under oscillating area conditions. *J. Colloid Interface Sci.* 229:353–364, 2000.

[16]Lambert, R. K., T. A. Wilson, R. E. Hyatt, and J. R. Rodarte. A computational model for expiratory flow. *J. Appl. Physiol. Respir. Environ. Exerc. Physiol.* 52:44–56, 1982.

[17]Otis, D. R., E. P. Ingenito, R. D. Kamm, and M. Johnson. Dynamic surface tension of surfactant TA: experiments and theory. *J. Appl. Physiol.* 77(2681–2688):1994, 1985.

[18]Rogers, D. F. Airway mucus hypersecretion in asthma: an undervalued pathology? *Curr. Opin. Pharmacol.* 4:241–250, 2004.

[19]Slutsky, A. S. Lung injury caused by mechanical ventilation. *Chest* 116:9S–15S, 1999.

[20]Tai, C.-F., S. Bian, D. Halpern, Y. Zheng, M. Filoche, and J. Grotberg. Numerical study of flow fields in an airway closure model. *J. Fluid Mech.* 677:483–502, 2011.

[21]Tawhai, M. H., A. Pullan, and P. Hunter. Generation of an anatomically based three-dimensional model of the conducting airways. *Ann. Biomed. Eng.* 28:793–802, 2000.

[22]Verkman, A. Role of aquaporins in lung liquid physiology. *Respir. Physiol. Neurobiol.* 159:324–330, 2007.

[23]Ware, L. B., and M. A. Matthay. The acute respiratory distress syndrome. *N. Engl. J. Med.* 342:1334–1349, 2000.

[24]Widdicombe, J. Regulation of the depth and composition of airway surface liquid. *J. Anat.* 201:313–318, 2002.

[25]Zheng, Y., H. Fujioka, S. Bian, Y. Torisawa, D. Huh, S. Takayama, and J. Grotberg. Liquid plug propagation in flexible microchannels: a small airway model. *Phys. Fluids (1994–present)* 21:071903, 2009.